Pacific Northwest
NATIONAL LABORATORY

PNNL-36607

Recycling of Titanium Scrap by Shear Assisted Processing and Extrusion (ShAPE)

September 2024

Scott A Whalen
Anthony P Reynolds
Devesh K Chouhan
Mageshwari Komarasamy
Brandon Scott Taysom
Nicole R Overman
Nathan L Canfield
Tim J Roosendaal

U.S. DEPARTMENT OF ENERGY

Prepared for the U.S. Department of Energy
under Contract DE-AC05-76RL01830

DISCLAIMER

PACIFIC NORTHWEST NATIONAL LABORATORY
operated by
BATTELLE
for the
UNITED STATES DEPARTMENT OF ENERGY
under Contract DE-AC05-76RL01830

Printed in the United States of America

Available to DOE and DOE contractors from
the Office of Scientific and Technical Information,
P.O. Box 62, Oak Ridge, TN 37831-0062
www.osti.gov
ph: (865) 576-8401
fox: (865) 576-5728
email: reports@osti.gov

Available to the public from the National Technical Information Service
5301 Shawnee Rd., Alexandria, VA 22312
ph: (800) 553-NTIS (6847)
or (703) 605-6000
email: info@ntis.gov
Online ordering: http://www.ntis.gov

PNNL-36607

0BRecycling of Titanium Scrap by Shear Assisted Processing and Extrusion (ShAPE)

September 2024

Scott A Whalen
Anthony P Reynolds
Devesh K Chouhan
Mageshwari Komarasamy
Brandon Scott Taysom
Nicole R Overman
Nathan L Canfield
Tim J Roosendaal

Prepared for
the U.S. Department of Energy
under Contract DE-AC05-76RL01830

Pacific Northwest National Laboratory
Richland, Washington 99354

Abstract

Titanium and its alloys are used in the aviation and automobile industries due to their remarkable strength to weight ratio, but, commonly, machining loss is high with ~90 wt.% of the material being converted to scrap. Recycling post-consumer Ti scrap directly into solid bulk products is a potential solution for repurposing valuable material. Further, reducing or even eliminating fresh Ti sponge during recycling might lead to lower energy and greenhouse gas emissions. In this study, a solid-phase process known as friction extrusion was utilized to recycle Ti-6Al-4V machining chips into solid wires which could be used as feedstock in additive manufacturing. The friction consolidation technique was first used to convert chips with varying degrees of oxygen content into solid billets for its use as feedstock material in subsequent friction extrusion. The extrudates were fabricated above the beta transition temperature, which was achieved by selecting rotation rate and feed rate, to process the billets near 1000°C using a tungsten-lanthana extrusion die. This work presents the first occurrence of friction extruded titanium alloy wires. The effect of friction extrusion on microstructural features, tensile properties, and texture are reported. Overall, the friction extrusion method is capable of recycling Ti-6Al-4V scrap directly into extruded wire.

Acknowledgments

This research was supported by the Solid Phase Processing Science Initiative (SPPSi) and Technology Deployment Office I3T Program at the Pacific Northwest National Laboratory (PNNL). The authors express appreciation for the excellent work performed by Anthony Guzman (PNNNL) on sample preparation and Daniel Wilhelm (University of South Carolina) on chip consolidation. Pacific Northwest National Laboratory is operated by Battelle Memorial Institute for the United States Department of Energy under contract DE-AC05-76RL01830.

1.0 Introduction

Titanium (Ti) and its alloys are used in aerospace, automobile, petrochemical, construction, and healthcare sectors due to their exceptional properties such as specific strength, toughness, biocompatibility, and resistance to oxidation [1]. Traditional machining operations are used to produce components, which may result in up to ~90 wt.% material loss as swarf during machining of a typical component. For example, Boeing uses around 120 tons of Ti alloy to build the 787 airframe, out of which ~83 wt.% or 100 tons of metal swarf is produced as scrap [2]. Ti is one of the most expensive structural materials because of the costly extraction and manufacturing of Ti sponge and difficult downstream processing [3]. To fulfill demand for defense, power generation, aviation and chemical industries, about $\$420$ million was expended by the U.S. to import Ti sponge in 2023, which is $\sim 54\%$ higher compared to 2022 [4]. In 2023, the U.S. imported nearly 26,000 tons of Ti scrap (wrought and cast) from the international market for recycling and other industrial utilization. Current recycling approaches require that Ti scrap be diluted with ~50% fresh Ti sponge to manage oxygen content. Reducing reliance on Ti sponge through direct recycling of swarf would conserve natural resources and the embodied energy and carbon associated with Ti extraction and production. Remelting of Ti swarf from traditional recycling requires process intensive techniques, including vacuum arc melting, induction skull melting and hydrogen plasma arc melting [5]. The melting process removes most volatile impurities but cannot separate out the nonvolatile metal impurities. Molten Ti has affinity for oxygen, nitrogen, and Fe transferred from the furnace and ladle, which lowers the quality of recycled Ti ingots [6]. As a result, scrap from high priced wrought Ti alloy turn into down-graded titanium ingot, which is used as feedstock material in the ferrotitanium industry. Overall, recycling Ti scrap via remelting is not only energy inefficient but also leads to the waste of high-priced metals. An alternate method for recycling machining swarf direct into a useful form without re-melting would be an advancement and is the subject of this work.

To bypass the melting step during recycling of metal scrap, severe plastic deformation (SPD) techniques such as hot and cold compression, spark plasma sintering (SPS), equal channel angular pressing (ECAP), continuous extrusion-forming (Conform), friction extrusion (FE), high-pressure torsion (HPT), and cyclic die oscillations were developed and utilized to overcome the drawbacks associated with remelting [7-11]. Application of large plastic strain, and high pressure at elevated temperature are required to break oxide layers on the swarf surface and to initiate diffusion bonding processes [7]. For instance, Tekkaya et al. [12] reported the recycling of aluminum (Al) 6060 machining scrap where the chips were pre-compacted into a cylindrical billet and then extruded using conventional direct extrusion at high temperature. Liang et al. [13] recycled magnesium alloy AZ91D chips by cold pressing into a cylindrical mold followed by hot direct extrusion to produce an 8 mm bar. These hot extrusion methods were aimed at breaking down the oxide layer to enable bonding between fresh metal surfaces. Whalen et al. [14] fabricated 5 mm diameter rods directly from gas-atomized aluminum transition metal powders by friction extrusion. The bulk nanostructured Al extrudates exhibited $\sim 380\, MPa$ yield strength, $\sim 450\, MPa$ ultimate tensile strength, and $\sim 15.7\,\%$ elongation at ambient temperature which is superior to the same alloy processed by traditional hot extrusion

[15]. Investigations by Lui et al. [7], Luo et al. [16], and Shi et al. [17] used ECAP to recycle various grades of Ti chips. Prior to ECAP, the metal chips were consolidated into cylindrical bars with a diameter of $\sim 10\ mm$ and length of $\sim 70\ mm$ by a hydraulic press. Thereafter, the consolidated chips were wrapped in metal foil, and subjected to up to eight ECAP passes at a temperature of $\sim 500℃$ with $100\ MPa$ back-pressure and the billet rotated $90°$ clockwise around the billet axis after each pass [17]. Similarly, Lui et al. [7] performed ECAP on compacted Ti-6Al-4V (Ti64) chips with up to 4 passes with the billet rotated $180°$ around the billet axis after each pass. It was observed that the selected pressure-temperature conditions were not sufficient to break the surface oxide nor evenly disperse the oxide throughout the microstructure, which resulted in ~11% ductility. From these investigations, it can be ascertained that recycling of Ti scrap via solid-state processes is feasible but depends on the quality or grade of scrap; in the cited works Ti chips were specially prepared via dry milling of bulk Ti alloy to avoid contamination. However, industry typically utilizes coolants during machining to improve the surface finish and tool life which results in contamination with volatile and non-volatile material.

In this work, friction consolidation is utilized to compact oxidized Ti64 swarf into a billet and friction extrusion is then employed to fabricate wires from consolidated billets. The aim of the present work is to develop the methodology and processing parameters for direct extrusion of Ti64 by friction extrusion. It should be noted that literature related to solid-state recycling of Ti alloys is scarce; moreover, the recycling techniques in the referenced literature employed multiple steps to process contamination free Ti scrap. The implementation of friction extrusion using a direct extrusion configuration for recycling of oxidized Ti64 swarf has not yet been reported in the literature.

2.0 Materials and Methods

The material used in this investigation was Ti64 alloy in the form of extruded bar and machined chips. The chips were prepared by machining a wrought Ti64 alloy via turning on a lathe. In this study, extrusion billets were prepared from three types of feedstocks: (i) extruded barstock, and friction consolidated (ii) non-heat-treated chips, (iii) and chips heat-treated at 400 ℃ for ~1 hr to intentionally increase oxygen content.

Figure 1a illustrates a schematic diagram of the friction consolidation apparatus to convert Ti64 chips (Figure. 1b) into consolidated billets for subsequent friction extrusion (Figure. 1c). The setup consists of four main parts: consolidation tool, billet chamber, backing plate and clamping/fixture. A Materials Test Systems (MTS) friction stir welder (FSW) was used to apply the necessary rotational and compression forces. A cylindrical consolidation tool with the dimension of $\Phi 19\ mm$ x 152 mm long was fabricated from Tungsten-1wt% Lanthana. The tool face was machined with a scrolled pattern having $\sim 4\ mm$ pitch, $\sim 0.5\ mm$ depth and $\sim 2.36\ mm$ land width to facilitate mixing and consolidation of the chips (Figure 1d). The backing plate and billet chamber are aligned concentrically with the rotating tool and clamped to the FSW machine table as shown in Figure. 1a. The billet chamber was partially filled with Ti chips (Fig.1b) and pre-compacted by applying 17.8 kN force. The tool was then retracted to ~0.5 mm above the compacted surface. At this stage, the tool rotation was brought to 450 RPM and the billet rammed against the rotating tool at rate of $1.3\ kN\ s^{-1}$ to achieve 22.2 kN. The chips were allowed to consolidate under extreme shear deformation for $\sim 50\ s$ time after which the tool was fully retracted from the chamber and rotation stopped. The process was repeated to achieve $\sim 45\ mm$ long consolidated billets. Consolidation was performed in an inert environment to limit further oxidation.

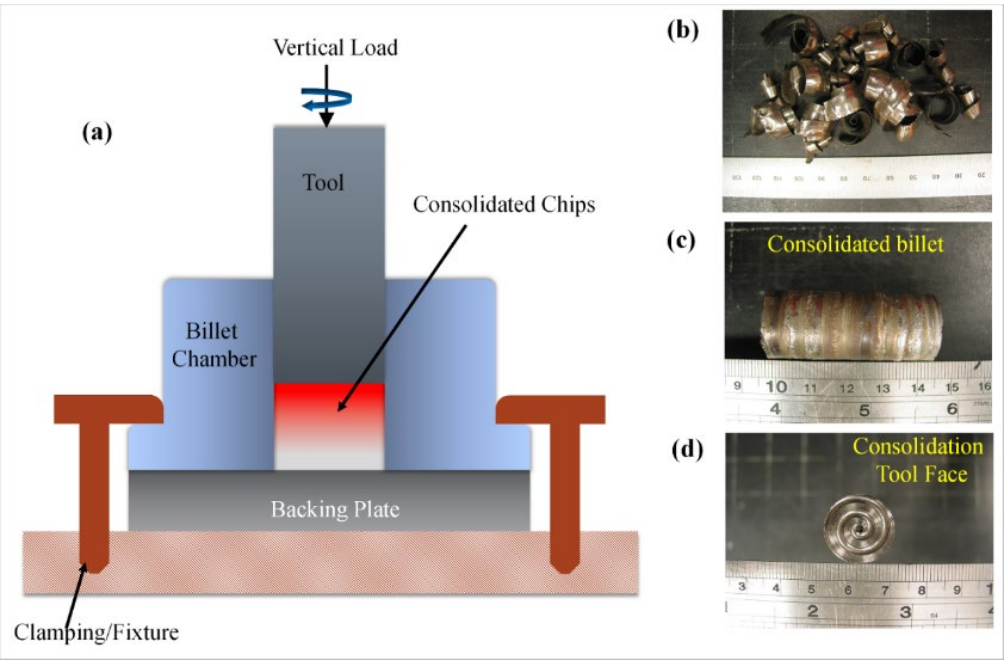

Figure 1 (a) Schematic diagram of friction consolidation apparatus, (b) Ti64 chips, (c) consolidated billet and (d) consolidation tool face with scrolled pattern.

A schematic of the direct friction extrusion configuration is shown in Figure 2a. In this configuration, the rotating tooling is held at a constant depth of 1 mm into the billet chamber while the consolidated Ti billet is rammed towards the rotating tool. Contact between the rotating tool and billet increases the interfacial temperature due to friction and adiabatic heating, which plasticizes the billet material. As interface temperature increases, billet material flows inward toward a 2.5 mm diameter extrusion orifice on the Tungsten-1wt% Lanthana tool face. Heat generation and deformation are regulated by adjusting rotating speed and ram speed, with motor torque and ram force following to reach the specified speeds. The direct extrusion configuration produces meters-long extrudates compared to the indirect configuration (Fig. 2b used in previous studies [18, 20] where extrudate length was limited by the tool length that could plunge into the container. The indirect approach also suffers from steadily increasing area of interaction along the tool outer diameter and billet chamber inner diameter where flash accumulates and creates unwanted frictional heating and torsional stress on the tool. Therefore, in this work friction extrusion in the direct configuration is used instead of indirect extrusion. Temperature of the tool face was measured using a K-type thermocouple within 0.5 mm of the face. Additionally, an argon cover gas was employed in the process region and where the extrudate exits the tool.

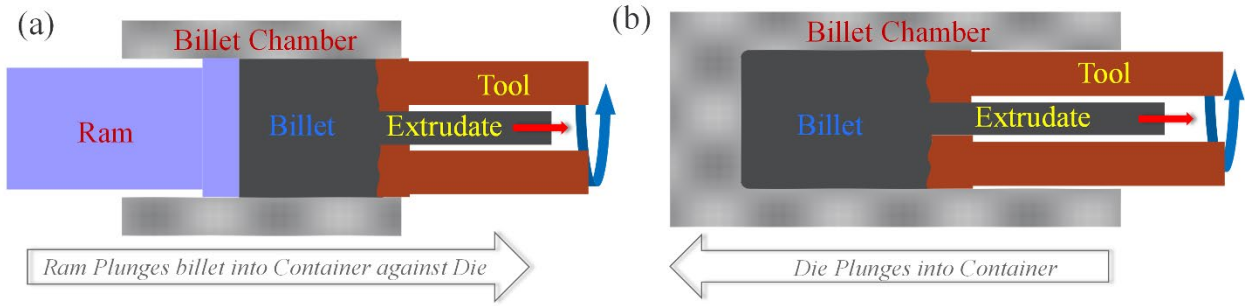

Figure. 2 Schematic of the (a) direct and (b) indirect configuration using friction extrusion.

The friction extrusion process primarily relies on three control parameters: (i) rotation speed, (ii) ram speed and (iii) tool geometry, which includes extrusion ratio. Initial trials were conducted on the wrought Ti64 feedstock to establish the appropriate rotation speed and ram speed for obtaining a tool face temperature around $980\ ℃$, which is close to the β –transition temperature (T_β). Typically, in conventional extrusion of Ti, areal extrusion ratios of $30{:}1$ [21] are employed at the β transition point. In these experiments, an extrusion ratio of 58:1 was utilized during friction extrusion. The extrusion speed is determined by multiplying extrusion ratio by ram speed. The ram force was determined by multiplying ram pressure by the cross-sectional area of the billet. The friction extrusion experimental parameters are given in Table.1. Figure 3 shows the experimental apparatus and a progression of improving extrudate surface quality as the inert argon (Ar) cover gas fixturing was refined.

Table 1. Friction extrusion process parameters used in this investigation.

ID No.	Feedstock material	Billet Diameter (mm)	Extrudate Diameter (mm)	Ram Speed $m\ min^{-1}$	Extrusion Speed (m/min)	Ram Force (kN)	Tool Face Temperature (°C)	Rotation Speed (rpm)
FE-1	Ti64 Wrought	19	2.5	0.020	1.16	90	985 ℃	236
FE-2	Ti64 Non-heat-treated Chips	19	2.5	0.020	1.16	90	980 ℃	236
FE-3	Ti64 Heat-treated Chips	19	2.5	0.020	1.16	90	990 ℃	236

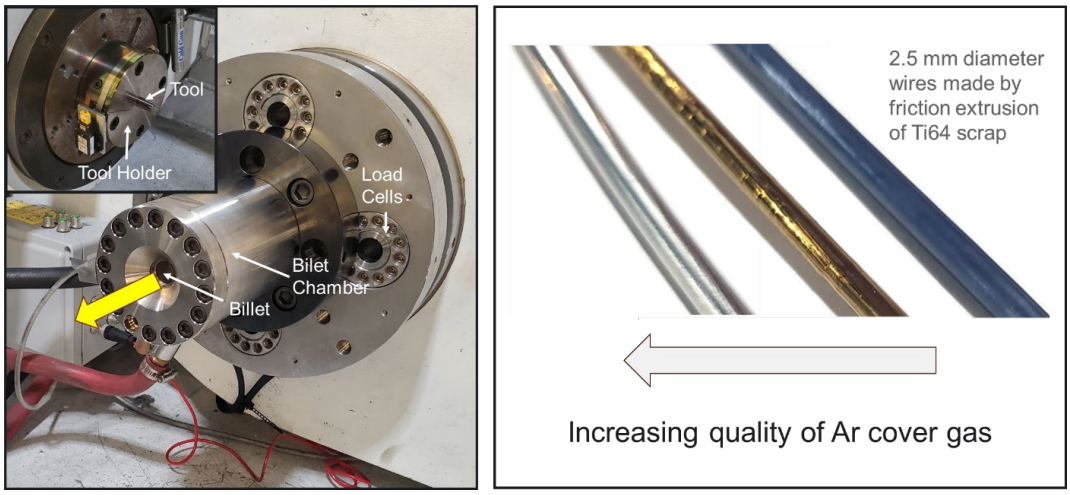

Figure 3. Friction extrusion apparatus (left) and exemplary 2.5 mm wires made by friction extrusion of Ti64 scrap (right).

Measurement of tensile properties was carried out using an MTS 22 kN servo hydraulic test frame in accordance with ASTM E8 guidelines for the wire specimens. Quasi-static uniaxial tensile tests were performed with displacement rate of 0.008 mm/s at room temperature and a laser extensometer was used to obtain the load versus displacement data. Three replicates were tested for each condition to determine the average values of yield strength (YS), ultimate tensile strength (UTS), and total elongation.

The extrudates were sectioned parallel to the extrusion direction (longitudinal), cold mounted, and polished using $\sim 0.05\ \mu m$ oil based colloidal silica. Quantitative microscopy and micro-texture data were captured using a JEOL 7600 Field Emission Scanning Electron Microscopy (FESEM) equipped with an electron backscatter diffraction (EBSD) detector. The instrument was operated with an accelerating voltage of 20kV, a working distance of 24 mm and a step size of $\sim 0.2\ \mu m$. The EBSD scans of $\sim 88 \times 65\ \mu m^2$ areas were performed on specimens from each extrusion condition and maintained the indexing rate above 90%. Further, the EBSD data were post processed and analyzed using AZtec Crystal 3.1.

3.0 Results

Fig. 4 shows the engineering tensile stress-strain plots of friction extruded samples made using the process parameters in Table 1. The average YS, UTS and total elongation (%) along with standard deviation are tabulated and shown within the Figure. It was observed that extrudates made from friction consolidated chips (FE-2 and FE-3) show higher tensile strength in comparison with the extrudate made from commercially available Ti64 barstock (FE-1). For comparison, the FE-1 extrudates exhibit $1030\ MPa$ YS, and $1170\ MPa$ UTS while FE-3 exhibits the greatest YS and UTS measuring $1295\ MPa$ and $1467\ MPa$ respectively. FE-2, made from non-heat-treated chips, exhibits intermediate behavior with YS and UTS measuring $1138\ MPa$ and $1258\ MPa$ respectively.

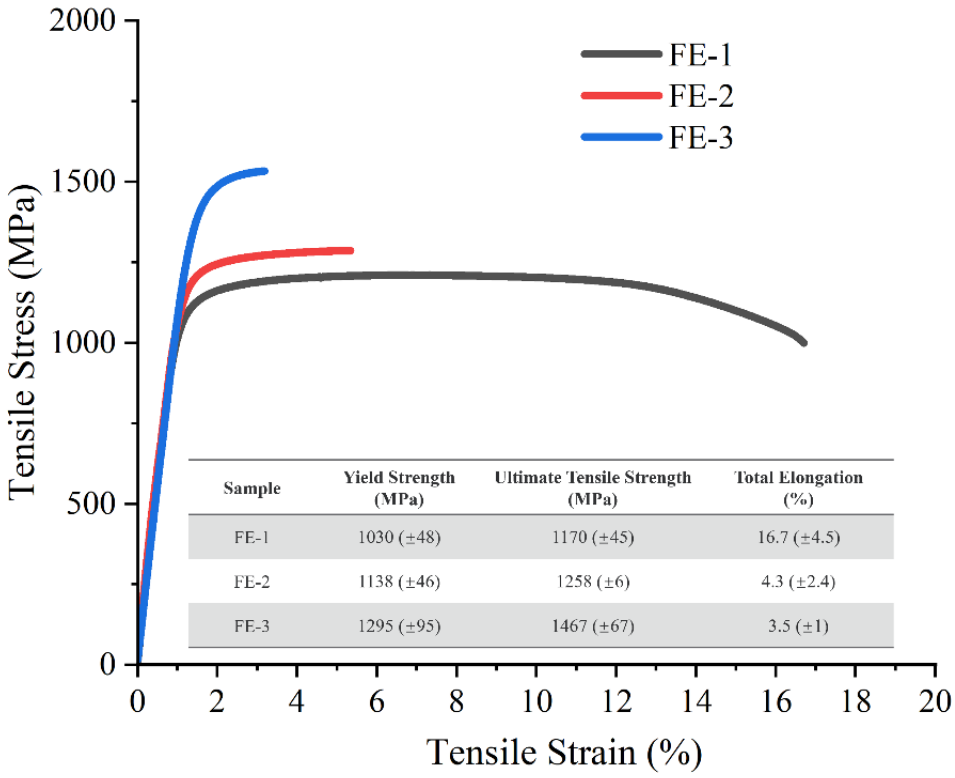

Sample	Yield Strength (MPa)	Ultimate Tensile Strength (MPa)	Total Elongation (%)
FE-1	1030 (±48)	1170 (±45)	16.7 (±4.5)
FE-2	1138 (±46)	1258 (±6)	4.3 (±2.4)
FE-3	1295 (±95)	1467 (±67)	3.5 (±1)

Figure. 4 Tensile stress vs tensile strain plots of processed samples with tabulated average YS, UTS and total elongation (%) along with standard deviation given in inset.

However, total % elongation reduces from ~16.7 % to 4.3%, to 3.5% for FE-1 compared to FE-2 and FE-3 respectively. According to the literature [22], the increase in strength in the case of processing the Ti64 below ($\leq 500℃$) could be associated with fragmentation and distribution of the oxide layer within the recycled material. However, processing of Ti64 above $500℃$, decomposes the oxide layer as oxygen starts to diffuse, occupying octahedral sites in the HCP lattice [23]. In this investigation, is it theorized that the combination of elevated temperature and extensive shear deformation results in the decomposition of oxides which increases the elemental oxygen content of the Ti matrix

specially in the case of FE-2 and FE-3. The excess amount of oxygen elements in Ti decreases the stacking fault energy of prismatic planes and alters the critical resolve shear stress (CRSS) values of prismatic, basal, and pyramidal slip systems [24,25]. Even though, the values of CRSSs associated with the various slips in Ti obtained from the crystal plasticity simulation, differ considerably [26,27], but there is common agreement that, CRSS of various slip systems under quasi-static deformation at ambient temperature are, $\mathrm{CRSS}_{\mathrm{prismatic}} < \mathrm{CRSS}_{\mathrm{basal}} < \mathrm{CRSS}_{\mathrm{pyramidal}}$. Therefore, the prismatic slip is the preferentially active slip system. However, the presence of excess oxygen atoms at octahedral sites within HCP lattice, increase the $\mathrm{CRSS}_{\mathrm{prismatic}}$ and $\mathrm{CRSS}_{\mathrm{basal}}$ more rapidly compared to $\mathrm{CRSS}_{\mathrm{pyramidal}}$, which means that large stresses are required to achieve elastic to plastic transition at room temperature.

Moreover, the presence of oxygen at octahedral sites of HPC lattice produces the non-isotropic lattice distortion and stretches the c–axis. Such lattice distortion induces the obstacle in dislocation glide which inhibits the ambient temperature twinning in material. The elastic strain field around the solute atom induces the compressive deformation, converts the glissile dislocation into a sessile dislocation, leading to a decrease in the overall ductility of material [22]. This could be one of the reasons for the limited ductility obtained in FE-2 and FE-3 samples during tensile testing.

Figure. 5 (a,b,c)-i illustrates the microstructure as inverse pole figure (IPF) maps for extrudates made by friction extrusion from the three feedstock materials in Table 1. IPF maps show a lamellar morphology (e.g., martensitic product), with different lath thicknesses in the extrudates. All extrusions were performed close to the β- transition temperature (tool face temperature was ~980-990°C) where β phase was present during extrusion. Upon cooling, the β phase converted into α-phase with lath morphology. The average thickness of laths in extrudates are typically $1.3 \pm 0.7\ \mu m$, $1.9 \pm 1.5\ \mu m$ and $2.7 \pm 1.6\ \mu m$ within FE-1, 2 and 3, respectively. Along with the thin α-laths structure, FE-3 shows a relatively large fraction of coarse α-phase (Fig. 5c-i) as compared to FE-1 and FE-2. The thickness and morphology of the α-laths depend upon the size of parent β grains, which is function of time spent at T_β. The parent β-phase IPF map is reconstructed using the parent grain analysis feature of AZtec Crystal. The reconstruction algorithm consists of three steps: (a) variant coalescence, (b) orientation refinement, and (c) regional voting. The detailed description of the orientation reconstruction is published by Huang et al. [29]. Reconstructed parent β-phase maps are shown in the Fig. 5 (a,b,c)-ii. The linear intercept approach is used to calculate the average grain size. The average grain size of β-phase was determined to be $18.8\ \mu m$, $21.5\ \mu m$, and $15.3\ \mu m$ in for FE-1, FE-2, and FE-3 respectively. The size of parent β grains in FE-1 and FE-2 extrudates are larger than FE-3. Heat treating chips (FE-2 and FE-3) results in the formation of additional surface oxide, which increases the total oxygen content in the billet used for FE-3. In Ti64, oxygen acts as an α-phase stabilizer that increases the T_β of Ti-alloy and helps to retain the α-phase at higher temperature [21,28]. Usually, the β-phase grain growth occurs with increasing temperature, in the absence of secondary phase, and excess elemental oxygen at octahedral sites in the HCP lattice, which typically impedes grain boundary motion [30, 24]. In this investigation, the presence of excess elemental oxygen in FE-3, may decrease β-phase grain growth compared to the other two feedstock materials.

Overall, the friction extrusion process was performed close to T_β and, considering the cubic and hexagonal crystal symmetry, during cooling a single β orientation would be transformed into the twelve α-phase orientations according to literature [31]. The parent and child orientation have a specific crystallographic orientation relation also known as Burger's orientation relationship, that is $\{110\}_\beta \parallel (0001)_\alpha$ and $\langle 111\rangle_\beta \parallel \langle 11\bar{2}0\rangle_\alpha$ [31].

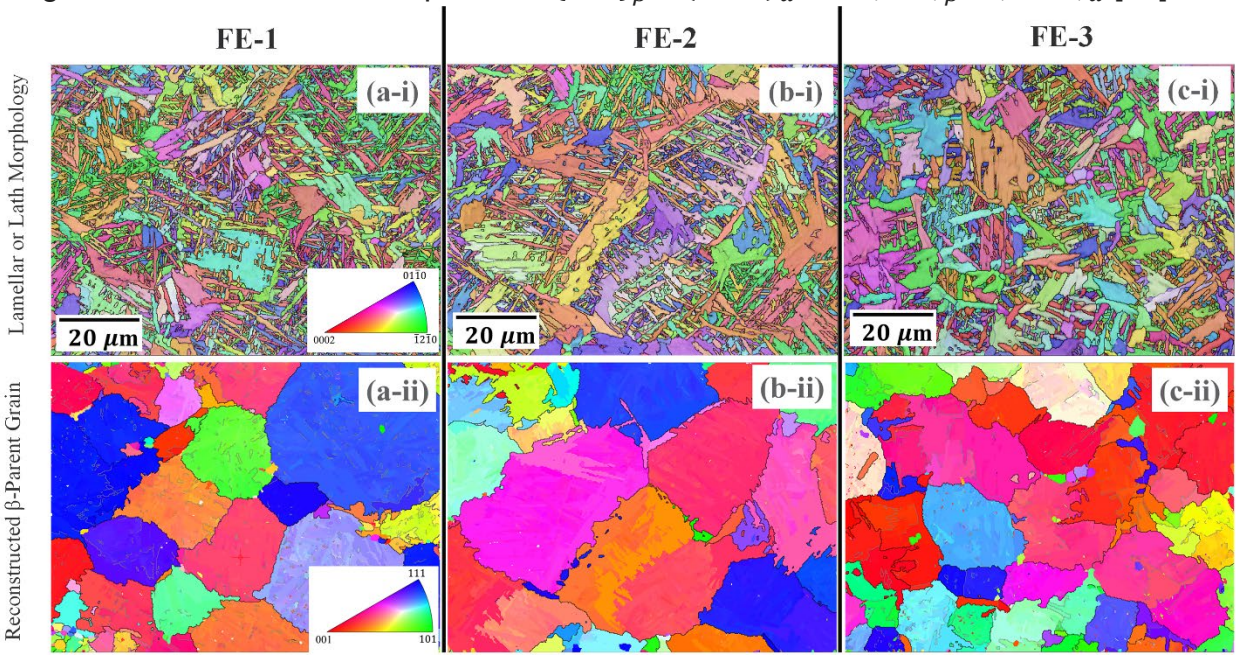

Figure 5. Inverse pole figure maps of FE-1 (a-i), FE-2 (b-i) and FE-3 (c-i) of Ti64 samples made by friction extrusion from the three feedstocks as per Table.1; corresponding reconstructed parent β grains in FE-1 (a-ii), FE-2 (b-ii), and FE-3 (c-ii) extrudates.

According to the literature [32], five distinct misorientation pairs are typically formed due to variant interactions. Fig. 6 shows misorientation angular distribution (MAD) plots for FE-1, FE-2 and FE-3. The plots illustrate three distinct peaks in the angular ranges of $\sim 5° - 15°$, $\sim 55° - 70°$, and $\sim 85° - 95°$. The corresponding angular inverse pole figures are plotted in Fig. 4d. There are five types of α/α inter-variant boundaries: Type I $\langle 0001\rangle/10.53°$, Type II $\langle 11\bar{2}0\rangle/60°$, Type III $\langle \overline{1.37}\ \bar{1}\ 2.37\ 0.359\rangle/60.83°$, Type IV $\langle \overline{10}\ 5\ 5\ \bar{3}\rangle/63.26°$ and Type V $\langle 1\ \overline{2.38}\ 1.38\ 0\rangle/90°$, respectively. In FE-1 and FE-2, Type II, III and IV α/α inter-variant boundaries are prominent.

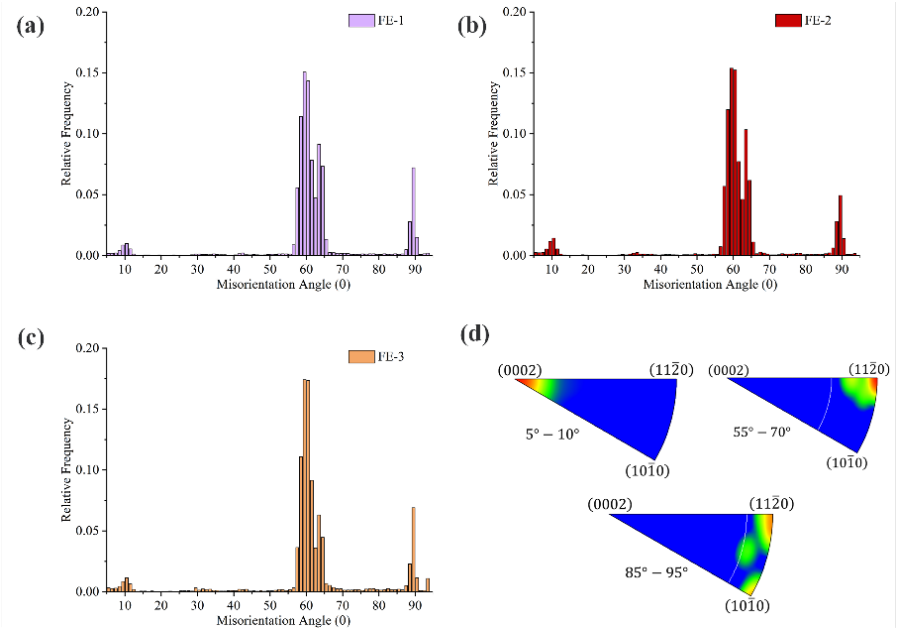

Figure 6. Misoreintation angle distribution plots extrudaes (a) FE-1, (b) FE-2, (c) FE-3, and (d) Angluar inverse pole figure correponding to $\sim 5° - 15°$, $\sim 55° - 70°$, and $\sim 85° - 95°$.

In FE-3, the relative frequency distribution of α/α inter-variant Type II, and III boundaries are identical to FE-1 and FE-2, except for Type IV, which has comparatively smaller fractions. Other types α/α inter-variant boundaries are also present in all three samples. Higher fraction of the inter-variant boundaries increases the required stress for plastic deformation and enhances the strain hardening response of material [33]. Kadiri et al. suggested that the evolution of multi-twin variants and their interaction boundaries significantly increases the isotropy and weakens the texture [34]. Microstructures with large fraction of coincidence site lattice boundaries (CSLBs) act as an effective obstacle for gliding dislocation and cause them to accumulate, improving the yield strength as well as the strain hardening behavior of material [35].

Although oxygen is the likely cause of reduced ductility, the mechanical properties are susceptible to many other microstructure features such as those in the preceding discussion making it challenging to identify the specific cause of limited ductility in the recycled Ti64 extrudates.

4.0 Conclusions

1. Ti64 chips were converted into billets by friction consolidation and subsequently extruded into ~2 to 2.5 meters-long wires using the friction extrusion process. Chips were utilized as machined and after heat treating at 400°C to intentionally increase oxide content.

2. All extrudates were processed close to the β −transition temperature; therefore, a transformed microstructure formed. Microstructures displayed five types of α/α inter-variant boundaries: Type I $\langle 0001\rangle/10.53°$, Type II $\langle 11\bar{2}0\rangle/60°$, Type III $\langle \overline{1.37}\ \bar{1}\ 2.37\ 0.359\rangle/60.83°$, Type IV $\langle \overline{10}\ 5\ 5\ \bar{3}\rangle/63.26°$ and Type V $\langle 1\ \overline{2.38}\ 1.38\ 0\rangle/90°$, respectively.

3. All extrudates demonstrated exceptional mechanical strength with FE-3 exhibiting the highest yield strength and ultimate tensile strength, measuring $1295\ MPa$ and $1495\ MPa$ respectively but with limited ductility of 3.5%

4. Refined lath type morphology occurs in all extrusions. The average lath thickness was found to be $1.3 \pm 0.6\ \mu m$, $1.9 \pm 1.5\ \mu m$ and $2.7 \pm 1.6\ \mu m$ in FE-1, FE-2 and FE-3, respectively.

5. The process induced temperature (β −transition temperature), and severe plastic deformation helped to decompose oxide and diffuse oxygen atoms in HCP lattice, which may lead to enhance the mechanical strength of FE-3 samples.

6. Friction extrusion was utilized to recycle Ti64 machining chips directly into extruded wire.

5.0 References

1. I.J. Polmear, Light alloys: Metallurgy of the light Metals, 4th ed. Butter-worth-Heinemann, 2006.

2. O. Takeda, T.H. Okabe, Current Status of Titanium Recycling and Related Technologies. JOM 2019, 71, 1981-1990.

3. D. Raabe, The Materials Science behind Sustainable Metals and Alloys. Chem. Rev. 2023, 123, 2436-2608.

4. U.S. Geological Survey (USGS), 2024, Mineral Commodity Summaries 2024: U.S> Geological Survey, 212 P.

5. B.M. Moon, J.H. Seo, H.J. Lee, K.H. Park, H.D. Jung, Method of Recycling Titanium Scraps via The Electromagnetic Cold Crucible Technique Coupled with Calcium Treatment. J. Alloys Compd. 2017, 727, 931-939.

6. J. Chae, J.M. Oh, S. Yoo, J.W. Lim, Eco-Friendly Pretreatment of Titanium Turning Scraps and Subsequent Preparation of Ferro-Titanium Ingots. Korean J. Met. Mater., 2019, 57, 569-574.

7. E. W. Lui, S. Palanisamy, M. S. Dargusch, K. Xia, Effects of Chips Conditions on the Solid-State Recycling of Ti-64 Machining Chips. J. Mater. Process. Technol., 2016, 238, 297-304.

8. D.T. McDonald, E.W. Lui, S. Palanisamy, M.S. Dargusch and K. Xia, Achieving Superior Strength, and Ductility in Ti64 Recycled from Machining Chips by Equal Channel Angular Pressing. Metall. Mater. Trans. A, 2014, 45, 4089-4102.

9. S.A. Smythe, B.M. Thomas, M. Jackson, Recycling of Titanium Alloy Powders, and Swarf through Continuous Extrusion (Conform™) into Affordable wire for Additive Manufacturing. Metals, 2020, 10, 843-861.

10. K. Topolski, P. Ostachowski, Solid State processing of Titanium Chips by unconventional plastic working. J. Mater. Res. & Technol., 2021, 13, 808-822.

11. Z. Feng, S.A. David, V.K. Manchiraju, D.A. Frederick, W. Thomas, Friction Extrusion: Solid-State Metal Synthesis and Recycling in Sustainable Manufacturing. J. Min. Met. Mat. Soc., 2023, 75, 2962-2973.

12. A.E. Tekkaya, M. Schikorra, D. Becker, D. Biermann, N. Hammer, K. Pantke, Hot profile extrusion of AA-6060 Aluminum Chips. J. Mater. Process. Technol., 2009, 209, 3343-3350.

13. M.L. Hu, Z.S. Ji, X.Y. Chen, Q.D. Wang, W.J. Ding Solid-state recycling of AZ91D Magnesium alloy chips. Trans. Nonferrous Met. Soc. China, 2012, 22, 68-73.

14. S. Whalen, M. Olszta, C. Roach, J. Darsell, D. Graff, Md. R. E. Rabby, T. Roosendaal, W. Daye, T. Pelletiers, S. Mathaudhu, N. Overman, High Ductility Aluminum Alloy Made from Powder by Friction Extrusion. Materialia, 2019, 6, 100260.

15. T. Wang T, B. Gwalani, J. Silverstein, J. Darsell, S. Jana, T. Roosendaal, A. Ortiz, W. Daye, T. Pelletiers, S. Whalen, Microstructural Assessment of a Multiple-Intermetallic-Strengthened Aluminum Alloy Produced from Gas-Atomized Powder by Hot Extrusion and Friction Extrusion. Materials, 2020, 13(23), 5333.

16. P. Luo, H. Xie, M. Paladugu, S. Palanisamy, M.S. Dargusch, K. Xia, Recycling of Titanium machining chips by sever plastic deformation consolidation. J. Mater. Sci., 2010, 45, 4606-4612.

17. Q. Shi, Y.Y. Tse, R.L. Highinson, Microstructure and texture development during solid consolidation recycling of Ti-6Al-4V. Mater. Chara., 2019, 147, 223-232.

18. S. Whalen, M. Olszta, Md. R-E-Rabby, T. Roossendaal, T. Wang, D. Herling, B. S. Taysom, S. Suffield, N. Overman, High Speed Manufacturing of Al alloy 7075 tubing by Shear Assisted Processing and Extrusion (ShAPE). J. Manuf. Process., 2021, 71, 699-710.

19. X. Li, D. Baffari, A.P. Reynolds, Friction Stir Consolidation of Aluminum Machining Chips. Int. J. Adv. Manuf. Technol., 2018, 94, 2031-2042.

20. B.K. Milligan, X. Ma, B.S. Taysom, S. Whalen, Solutionization via Severe Plastic Deformation: Effect of Temperature and Quench Method in a ShAPE-Processed Al-Mg-Si Alloy. Metall. Mater. Trans. A, 2023, 54, 2576-2584.

21. F.H. Froes, Titanium: Physical Metallurgy, Processing, and Applications, ASM Handbook, ASM International, 2015.

22. Conrad et al. 1981, Effect of interstitial solutes on the strength and ductility of Titanium, Prog. Mater. Sci., 26, 1981, 123-403.

Pacific Northwest National Laboratory

902 Battelle Boulevard
P.O. Box 999
Richland, WA 99354

1-888-375-PNNL (7665)

www.pnnl.gov